Arab J Sci Eng (2016) 41:1199–1213
DOI 10.1007/s13369-015-1817-4

RESEARCH ARTICLE - CIVIL ENGINEERING

Comparison of Local Scour Characteristics around Two Eccentric Piers of Different Shapes

Subhasish Das[1] · **Rajib Das**[1] · **Asis Mazumdar**[1]

Received: 2 August 2014 / Accepted: 10 August 2015 / Published online: 4 September 2015

Abstract Local scour at single pier has been extensively studied by several investigators, but scanty work is available on scour around piers placed in close proximity. The present research is concerned with experimental studies of the formation and characteristics of local equilibrium scour around a set of two identical circular-, square-, and triangular-shaped piers placed in longitudinal direction to the flow with a constant eccentricity (transverse distance). The objective is to see the nature of scour evolved due to the effect of mutual interference of one pier on another with the longitudinal spacing between them varying 0.25, 0.375, 0.5, 0.625, and 0.75 times the scour-affected lengths for a single-pier test. Analysis of the results shows the variations of individual non-dimensional equilibrium scour parameters with the effective pier width (diameter of the smallest circumscribing circle of the pier) and increasing longitudinal spacing between the piers.

Keywords Open-channel flow · Clear water scour · Eccentric pier · Characteristic pier width · Longitudinal spacing

✉ Subhasish Das
subhasishju@gmail.com

Rajib Das
rajibdas79@gmail.com

Asis Mazumdar
asismazumdar@yahoo.com

[1] School of Water Resources Engineering, Jadavpur University, Kolkata 700032, West Bengal, India

Notations

a_c	Characteristic cross-sectional area of pier inside the water (cm^2), πb_c^2
a_p	Cross-sectional area of pier (cm^2), πb^2
a_s	Planner surface area of equilibrium scour hole (cm^2)
b	Pier diameter or width (cm)
b_c	Characteristic pier width (cm), $b_e K_s$
b_e	Effective pier width (cm)
d_{se}	Equilibrium scour depth (cm)
d_s	Maximum equilibrium scour depth (cm)
d_{50}	Median diameter of sand (mm)
e	Center-to-center distance between the front and rear piers (cm), $3b$
F	Froude number of flow, $U/\sqrt{gh}$
h	Approaching flow depth (cm)
K_s	Ratio of the scour depth for any pier to that for the circular pier
l	Longitudinal spacing (along the flow) between the front and rear piers (cm)
l_{sm}	Maximum equilibrium scour length for two-pier arrangement (cm)
l_{sn}	Maximum net scour length for two-pier arrangement (cm), $l_{sm} - l$
l_{ss}	Maximum equilibrium scour length for single pier (cm)
L	Maximum equilibrium length of sediment transportation (cm)
r	Correlation coefficient
R	Hydraulic radius (cm)
R_e	Flow Reynolds number, UR/ν
R_p	Pier Reynolds number, Ub/ν
u_c	Critical velocity (cm/s)
u_*	Shear velocity (cm/s)
U	Depth-averaged approaching flow velocity (cm/s)

$\forthv_c$	Characteristic volume of pier below the water surface level (cm^3)
$\forthv_p$	Volume of pier below the water level (cm^3), $d_{sm}a_p$
$\forthv_s$	Volume of equilibrium scour hole (cm^3)
w_{sm}	Maximum scour width for two-pier arrangement (cm)
w_{ss}	Maximum scour width for single pier (cm)
ρ	Mass density of water (kg/m^3)
ρ_s	Mass density of sand (kg/m^3)
σ_g	Geometric standard deviation, $\sqrt{d_{84}/d_{16}}$
ν	Kinematic viscosity (m^2/s)
φ_r	Angle of repose (deg)

1 Introduction

Local scour phenomena are common in many hydraulic structures. A large number of studies have been conducted to predict the scour depth in the base of bridge piers by many researchers [1–12]. These studies have been performed primarily by means of laboratory-flume experiments, including the use of dimensionless equations finally resulting in some semiempirical equations for the maximum scour depth. A long-standing concern is the tendency of some of these equations to overpredict the maximum scour depth for field or even for laboratory conditions [12–14]. Most of these studies have been confined to single piers.

Also due to geotechnical and economical reasons, bridge designs often lead to complex piers or pier groups [15–18], in which case the direct application of the results derived from single piers may be problematic.

Nowadays, new bridges are constructed beside an existing bridge to meet the increasing demand of transportation for different kinds of vehicles. Sometimes a pier of the new bridge is positioned downstream eccentrically with respect to the pier of the existing old bridge. It is like a two-pier arrangement with the rear pier placed eccentrically with respect to the front pier. The developed horseshoe vortex of the eccentric rear pier comes in contact with the developed wake vortex of the front pier. The combined strength of both vortices increases scour hole around the rear pier, thereby increasing the rate of sediment transport. The suitability and effectiveness of this kind of natural occurrence with particular reference to enhancement of sediment transport may be explored as a desilting mechanism in future.

Despite a large number of investigations (as mentioned earlier) around single piers, a comprehensive understanding of scour geometry around pier groups and complex piers with eccentric arrangement [18,19] is still deficient because most of the pier group investigations have been confined to side-by-side and in-line arrangements that focused on the prediction of the scour geometry [7,16,17,20,21] and the effect of pier spacing on scour depth [22–24].

Sometimes a new bridge is constructed beside an existing bridge to make available an alternate route for traffic. Here a single pier of the new bridge is situated eccentrically downward from a single pier of the old bridge. It was explained how eccentrically arranged piers can cause sediment to move toward the river bank flowing downstream [15]. The horseshoe vortex in the middle of two piers can increase the scour hole of the downstream pier while shifting the sediments away from the downstream plane of symmetry. The suitability and efficiency of this kind of natural phenomenon with a particular reference to enhancement of scour may also be explored to use it as an alternative to self-dredging.

It appears from the literature survey that almost no experimental work was carried out to study the scour hole geometry around the pier, in case the piers were placed in eccentric arrangement with varying longitudinal spacing (spacing along the flow). Therefore, engineering solutions, concerning especially selection of scour countermeasures and their placement details, would be subject to uncertainty. To offset this problem, additional experimental studies need to be conducted. In the present study, an attempt has been made to carry out experiments with eccentric arrangement of pier groups varying the longitudinal spacing and to delineate the scour geometry.

2 General Experimental Technique

The experimental setup and conditions of the work are described in detail with the help of the schematic diagrams as shown in Fig. 1a–c. All tests were conducted in the Fluvial Hydraulics Laboratory of the School of Water Resources Engineering in Jadavpur University, Kolkata, West Bengal, India. Experimental conditions are explained in Table 1.

All the 19 tests conducted here were carried out with two identical piers of eccentricity e equal to a three times pier width ($e = 3b$) by because this is the maximum permissible limit [19] for piers that are 7 cm wide within which the equilibrium scour formed was expected to remain independent of the wall effects of the laboratory flume having a width of 0.81 m. For pier width less than or equal to 7 cm, the equilibrium scour formed was expected to remain independent of the wall effects of the laboratory flume having a width of 0.81 m [25–27]. The tests were carried out in a re-circulating tilting flume 11 m long and 0.6 m deep. The working section of the flume was filled with sand to a uniform thickness of 0.2 m. The length of the sand bed was 3 m, and its width was 0.81 m. The sand bed was located 2.9 m downstream from the flume inlet to make the fully developed flow. The re-circulating flow system was served by a 10-hp variable speed centrifugal pump with a maximum discharge of 25.5 L/s. The water discharge was measured by a flow meter connected to the upstream pipe at the inlet of the flume.

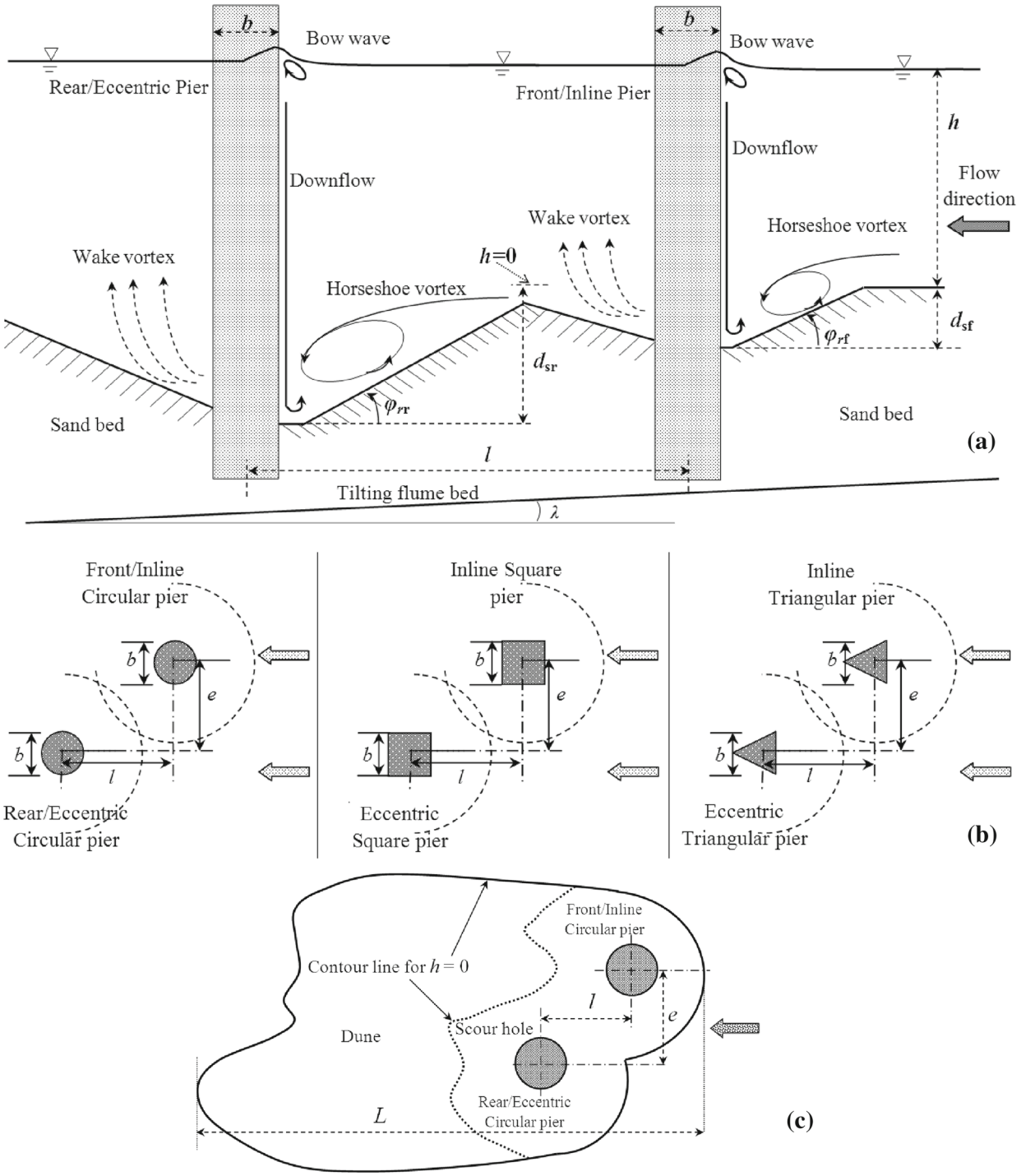

Fig. 1 **a** Schema of flow pattern and local scour around two eccentric piers, **b** *horizontal planes* for the measurements of scour geometry at different piers and **c** *horizontal plane* for gauge reading for circular pier

A movable trolley with a vernier point gauge attached to it was placed on the flume. A vertical scale was fixed with the point gauge to measure the water level, initial bed level, and scour depth. Perspex-made piers were placed in the middle of the working section of the flume. All tests were conducted using one sand bed material. The bed material (sand particles) size was: d_{50}(=0.73 mm), d_{16}(=0.5 mm), d_{84}(=1.42 mm), and d_{90}(=1.58 mm), which were measured from the sieve analysis test using a vibrating shaker. Geometric standard deviation of sediment size σ_g, given by $\sqrt{d_{84}/d_{16}}$, was equal

Table 1 Dissimilarities of experimental conditions and magnitudes of geometrical scour parameters for all tests

Test No.	b (cm)	Pier shape	l (cm)	t (h)	L (cm)	b_e (cm)	d_{ss} (cm)	d_{sf} (cm)	d_{sr} (cm)	b_{cf} (cm)	b_{cr} (cm)	l_{ss} (cm)	l_{sm} (cm)	w_{ss} (cm)	w_{sm} (cm)	a_s (cm^2)	$\forall_s$ (cm^3)
1	5	Circular	–	36	31.9	5	4.0	–	–	–	–	24.0	–	25.0	–	491.9	708.4
2	7	Circular	–	36	48.4	7	4.8	–	–	–	–	25.0	–	31.0	–	2082.2	864.1
3	7	Circular	$0.250L_2$	80	80	7	–	4.8	5.8	7.00	7.00	–	38.0	–	53.6	2960.0	1875.1
4	7	Circular	$0.375L_2$	80	90	7	–	5.4	6.2	7.00	7.00	–	44.5	–	54.7	3861.1	2576.8
5	7	Circular	$0.500L_2$	80	114	7	–	5.9	6.5	7.00	7.00	–	54.5	–	56.2	4372.7	3015.0
6	7	Circular	$0.625L_2$	85	128	7	–	6.2	6.7	7.00	7.00	–	62.5	–	57.0	4635.4	3406.9
7	7	Circular	$0.750L_2$	90	136	7	–	6.5	6.9	7.00	7.00	–	69.0	–	56.0	4833.4	3730.0
8	7	Square	–	42	66	9.9	5	–	–	–	–	28.5	–	31.8	–	2647.6	1065.7
9	7	Square	$0.250L_8$	80	96	9.9	–	5.3	6.6	10.93	11.26	–	44.0	–	56.9	4232.7	2093.8
10	7	Square	$0.375L_8$	80	104	9.9	–	5.9	7.2	10.82	11.50	–	52.5	–	60.0	5009.8	3258.6
11	7	Square	$0.500L_8$	83	126	9.9	–	6.4	7.6	10.74	11.57	–	64.0	–	64.2	5473.5	4030.6
12	7	Square	$0.625L_8$	87	142	9.9	–	6.6	7.9	10.54	11.67	–	75.5	–	67.5	5895.3	4763.5
13	7	Square	$0.750L_8$	95	153	9.9	–	6.7	8.1	10.20	11.62	–	85.0	–	64.5	5916.3	5183.2
14	7	Triangular	–	39	56	8.1	4.9	–	–	–	–	25.5	–	31.0	–	2176.3	1005.7
15	7	Triangular	$0.250L_{14}$	80	99	8.1	–	5.1	6.4	8.92	8.92	–	37.0	–	56.0	3981.1	1969.2
16	7	Triangular	$0.375L_{14}$	80	121	8.1	–	5.7	7.0	9.13	9.13	–	44.0	–	59.1	4854.8	2876.6
17	7	Triangular	$0.500L_{14}$	80	132	8.1	–	6.0	7.4	9.20	9.20	–	53.0	–	62.6	5296.2	3508.4
18	7	Triangular	$0.625L_{14}$	85	141	8.1	–	6.3	7.7	9.29	9.29	–	65.0	–	64.5	5611.4	4119.8
19	7	Triangular	$0.750L_{14}$	92	147	8.1	–	6.6	7.9	9.25	9.25	–	73.0	–	61.1	5804.5	4645.6

t is the run duration for each test; effective pier width b_e is the diameter of the smallest circumscribing circle of the pier [26]; b_{cf} and b_{cr} are the characteristic pier widths of the front pier and rear pier, respectively, and are equal to $b_e K_{sf}$ and $b_e K_{sr}$, respectively, where K_{sf} and K_{sr} are the shape coefficients of the front and rear piers, respectively;d_{ss}, l_{ss}, and w_{ss} are the maximum equilibrium scour depth, length, and width for the single pier, respectively; d_{sf} and d_{sr} are the maximum equilibrium scour depths at the upstream of the front pier and rear pier, respectively; l_{sm} and w_{sm} are the maximum equilibrium scour length and width, respectively; a_s and $\forall_s$ are the planner surface area and volume of the equilibrium scour hole, respectively

to 1.68. It was proposed that the sediment can be considered as uniform when $\sigma_g < 2$ [23]. Therefore, the scour depths to be measured after the tests can reach their maximum clear water value. Relative density of the sand, angle of repose of the bed sediment in still water (φ_r), average bed shear stress, and critical bed shear stress [25–27] were measured as 2.582, 36°, 0.39, and 0.40 Pa, respectively. For all tests, flow velocity, Froude number of flow, flow Reynolds number, pier Reynolds number, and shear Reynolds number were measured as 0.247 m/s, 0.223, 24165, 17709, and 1340, respectively. The magnitude of shear Reynolds number indicates that the flow was fully turbulent.

Tests 1 and 2 were conducted to find out the maximum pier width (based on market availability) for which the transporting sand will not touch the flume's side wall during two-pier tests. Based on this concept, a pier width (b) of 7 cm was selected for tests 3–7 (circular), 9–13 (square), and 15–19 (triangular). The maximum equilibrium scour-affected length and longitudinal spacing between the in-line front and eccentric rear piers are denoted by L and l, respectively, as shown in Fig. 1c. For single-pier tests (2, 8, and 14), the maximum equilibrium lengths of sediment transportation were denoted by L_2, L_8, and L_{14}, respectively, and were found to be 48.4, 66, and 56 cm, respectively. Five different longitudinal spacings (l) were tested. The longitudinal spacing (l) considered was $0.25L_x$, $0.375L_x$, $0.5L_x$, $0.625L_x$, and $0.75L_x$ (where $x = 2$, 8, and 14 based on the shape of pier). From previous research, it was found that for two piers with the centerline gap of $3b$, the maximum scour depth increases by 20 % [7]. It was also observed that the ratio of eccentricity and pier width (e/b) is equal to seven as a limit for pier independency [22].

The approaching flow depth (h) was maintained as 12.5 cm by operating the tailgate. The bed slope (S) equal to 1:2400 was kept constant for all tests. The critical condition of the bed was verified before each test run as recommended by [26]. All tests were set up so that the approaching flow would have undisturbed flow depth where the ratio between the approaching flow depth and pier width (h/b) was 1.786. The depth-averaged approaching flow velocity U was set as 24.7 cm/s, which is about 68.2 % of the critical velocity u_c to satisfy the clear water ($U/u_c < 1$, [25–27]) scour condition. In order to observe the maximum clear water scour depth, it was explained that $U/u_c < 0.8$ when $d_{50} > 0.7$ mm [23].

The minimum total duration of each of the two-pier experiments was 80 h, which was considered adequate for achieving the equilibrium scour [9,25,27] as the scour depth increase for every 2 h was less than 1 mm. After each test run, the maximum equilibrium scour depth was observed at the upstream base of the in-line front and eccentric rear piers. Then the maximum equilibrium scour depths at an equilibrium state were carefully measured by a Vernier point gauge with an accuracy of ±0.1 mm gap. The dynamic angle of reposes for the in-line front pier (φ_{rf}) and eccentric rear pier (φ_{rr}) was measured to be about 12.5 and 10.5 % greater than the angle of repose of the bed sediment in still water (φ_r), respectively.

The equilibrium planer scour surface area (a_{se}) and scour volume ($\forall_{se}$) are computed for all the tests using Surfer Software which was also adopted by previous researchers [8,9]. This technique is capable of evaluating area and volume of scour holes bounded by contour. For the sake of practical applications, planner surface area of the equilibrium scour hole in non-dimensional form (a_{se}/a_c) and dimensionless scour volume ($\forall_{se}/\forall_c$) are defined in which a_c and $\forall_c$ are equal to characteristic area of the pier ($=\pi b_c^2$) and characteristic volume of the pier ($=ha_c$), respectively.

3 Results and Discussions

In case of two-pier in in-line position, the scouring mechanism affect around the front pier is reinforcing. It leads to increased scour depth at the front pier if the scour at the downstream pier overlaps with that at the front pier. The lowering of the bed level at the rear eases the escape of sediment from the scour hole and leads to deeper scour.

The photograph of scour-affected zones around the circular, square, and equilateral triangular piers is displayed in Fig. 2. The contour lines of the scour holes at the circular, square, and equilateral triangular piers, plotted with the Golden software Surfer version 8.06.39, are shown in Figs. 3, 4, and 5, respectively. Near about 600 points were measured with point gauge after each test and used to draw the contour lines. Table 1 summarizes the values obtained for the equilibrium scour parameters for all tests.

It can be seen from the contour diagrams (Figs. 3, 4, 5) that the scour hole is mostly continuous and there exists no deposition between the piers. Now it is important to know which combination of longitudinal spacing removes more sand from the bed for desilting purpose. To understand which combination of pier removes more sand, the scour depth below zero contour line was determined with the help of surfer software. Since one of the objectives here is to find out which combination of pier gives the maximum scour (not the exact scour volume), the scour depth below zero contour line is determined assuming that the scour hole volume below zero contour line will give a rough idea.

3.1 Dimensional Analysis

In the present research, the quantitative study is limited to the equilibrium scour depth reached by the scour hole around the pier after sufficient time has elapsed. Considering an isolated single pier in a rectangular tilting flume, where the flow

Fig. 2 Scour-affected zones around *circular*, *square* and *triangular* piers for *tests 1–19*

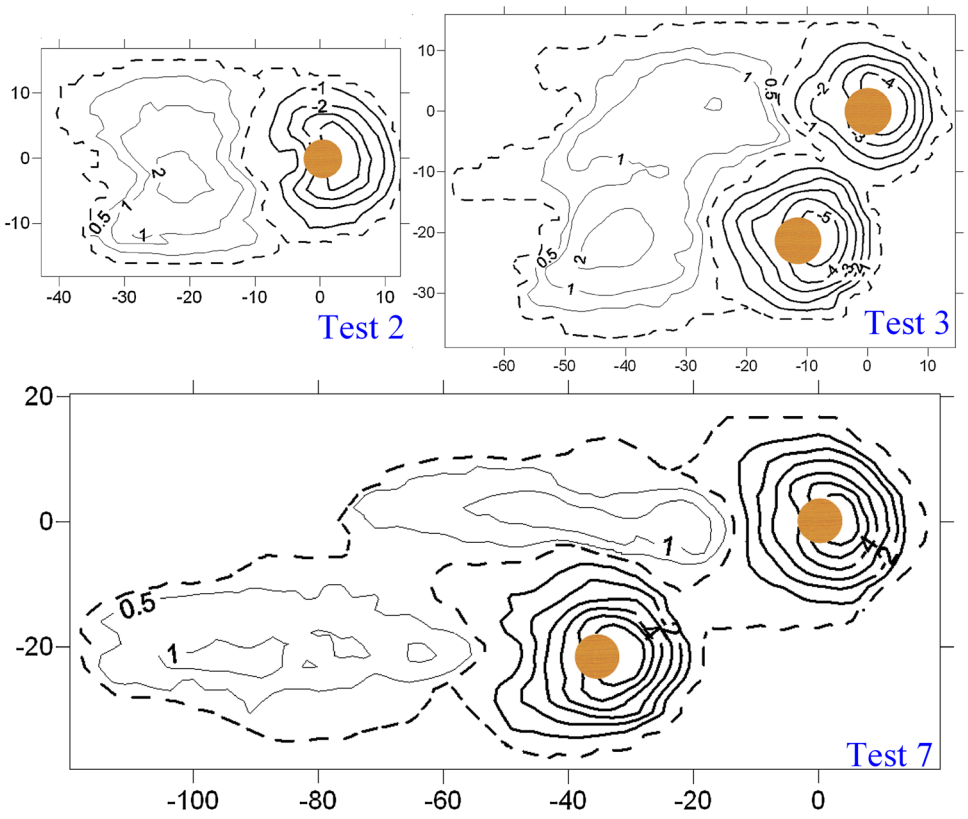

Fig. 3 Contours of equilibrium scour holes for *tests 2–7* (units: cm)

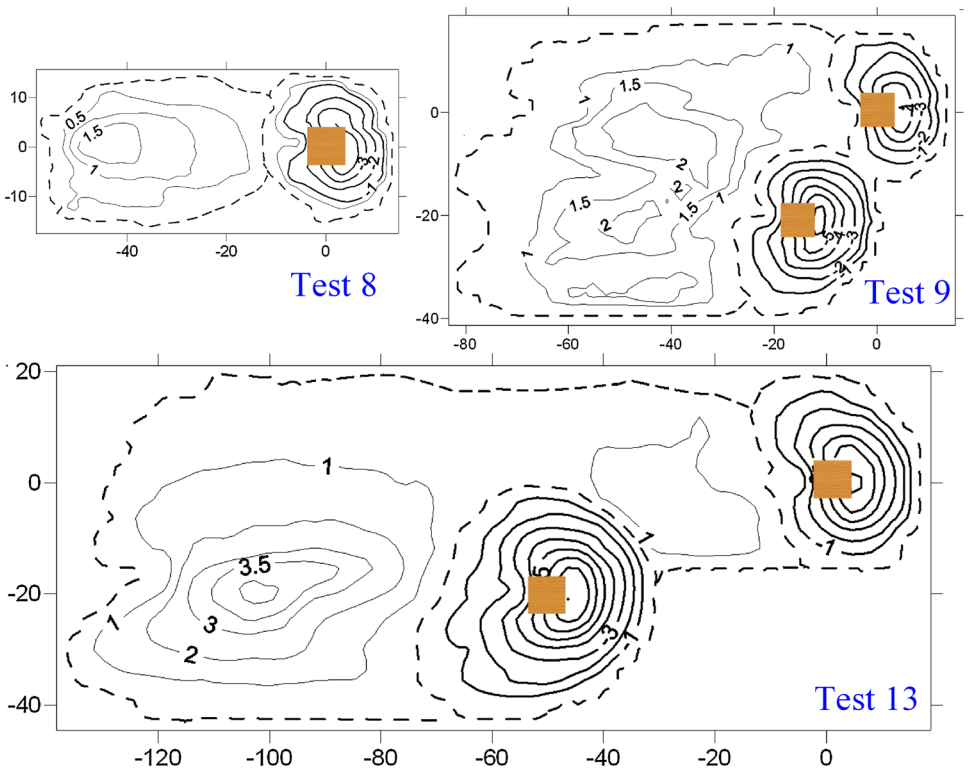

Fig. 4 Contours of equilibrium scour holes for *tests 8–13* (units: cm)

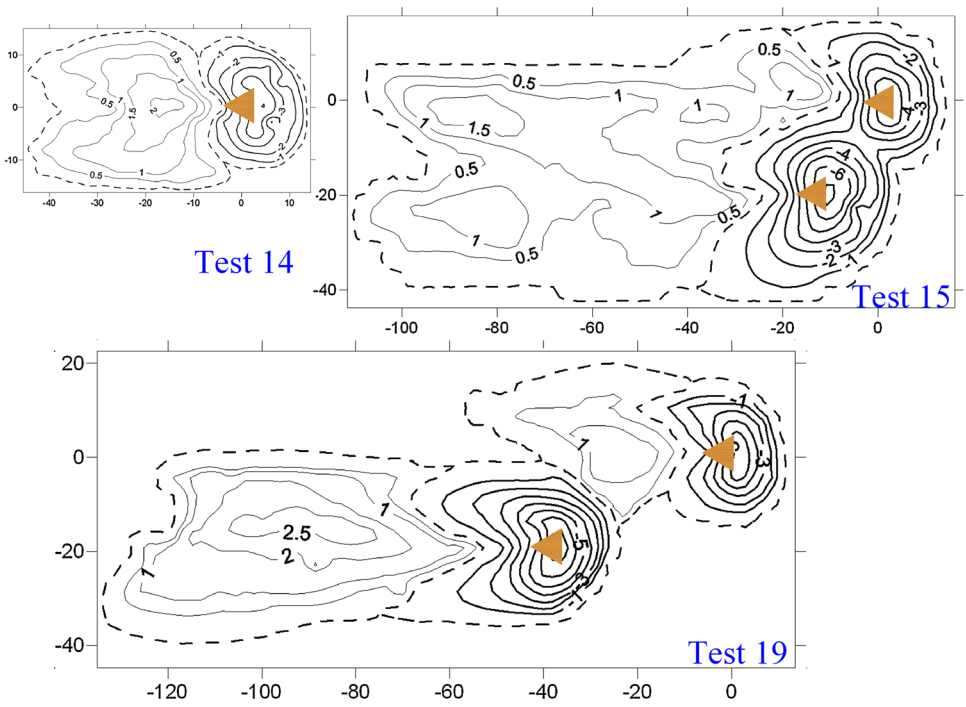

Fig. 5 Contours of equilibrium scour holes for *tests 14–19* (units: cm)

is unidirectional and whose bed is made up of cohesionless sand particles, the equilibrium scour depth depends on the water (density and viscosity), sand particles (density and median particle diameter), channel flow (flow depth, channel slope, and gravity) that is the depth-averaged velocity, and the geometry of pier (a characteristic pier width, pier-shape coefficient). For circular pier, the characteristic pier width b_c is same as the pier diameter [24]. Characteristic pier width $b_c = b_e K_s$, where b_e = effective pier width [28], i.e., diameter of the smallest circumscribing circle of the pier and K_s = pier-shape coefficient. The pier-shape coefficient K_s is defined as the ratio of the scour depth for a particular pier shape to that for the circular pier. Characteristic pier width b_c can be considered as a very important parameter since it takes into account both b_e and K_s.

In the present study, the densimetric Froude number, inflow depth, and pier Reynolds number have been kept constant and the variation of scour depth with respect to pier spacing, pier width and characteristic pier width is investigated.

The list of parameters is very long, and some of them are, moreover, difficult to quantify, such as the particle size distribution, the grain form, or the cohesion of the bed materials. For this reason, the analysis has been made mainly for the following restrictive conditions:

Bed material: the sediment is non-cohesive and has a uniform size d_{50}.

Flow: flume sufficiently wide so that the pier does not cause a significant contraction.

Pier: perfectly smooth.

The parameters which remain are:

- for the water: Mass density ρ; kinematic viscosity ν; and gravitational acceleration g;
- for the bed material: Median particle diameter d_{50}; and its density ρ_s;
- for the flow: Approaching flow depth h; depth-averaged inflow velocity of the undisturbed flow U or the shear velocity u_*, equal to $\sqrt{ghS}$;
- for the pier: its pier width b or characteristic pier width b_c; and
- for the pier spacing: Longitudinal spacing (spacing along the flow) between the front and rear piers l; and transversal spacing (eccentricity) between the front and rear piers e.
- In the present dimensional analysis, equilibrium scour depth d_{se} is the scour considered around any of the pier, i.e., front or rear.

Therefore, the equilibrium scouring depth d_{se} depends on 10 parameters:

$$d_{se} = f\,(\rho, \nu, \rho_s, d_{50}, h, u_*, g, b \text{ or } b_c, l, e) \tag{1}$$

The Vaschy–Buckingham π-theorem allows us to write:

$$\frac{d_{se}}{b} = f_0\left(\frac{u_* d_{50}}{\nu}, \frac{u_*^2}{\Delta g d_{50}}, \Delta, \frac{h}{b_c}, \frac{d_{50}}{b_c}, \frac{l}{b_c}, \frac{e}{b_c}\right) \tag{2}$$

The justification for the choice of the dimensionless groups is the following:

- d_{se}/b: Experiments have clearly demonstrated that it was possible to relate the scour depth to the diameter of the pier. This may be explained physically by the fact that the scouring process is governed by the downflow–horseshoe–wake vortex system whose dimension is a function of the diameter of the pier [1].
- $u_* d_{50}/\nu$, $u_*^2/\Delta g d_{50}$: These are classical parameters in the study of bed load. According to many studies, U/u_c is a predominant parameter for analysis of local scour around piers. But it is not considered in the dimension analysis as U/u_c is constant for all the tests.
- h/b_c, d_{50}/b_c: These ratios relate the size and shape of the pier to that of the flow and of the sand particles.

Equation (2) can be considerably simplified by the following considerations:

- The influence of kinematic viscosity ν is insignificant for a turbulent flow over rough beds [29].
- Shear velocity u_* was kept constant for all tests.
- In sediment-water interaction, the parameters g, ρ, and ρ_s were combined into one parameter, namely relative submerged weight, Δg given by $\{(\rho_s/\rho) - 1\}g$ [26]. The term $\Delta(=1.582)$ was also kept constant.
- The median particle diameter d_{50}, inflow depth h, depth-averaged inflow velocity U, and eccentricity e were kept constant for all tests. Therefore, these terms can be neglected.

Therefore, Eq. (2) can be written as,

$$d_{se}/b = f_1\,(l/b_c) \tag{3}$$

It implies that the relative maximum equilibrium scour depth (d_{se}/b) can be expressed in non-dimensional form as a function of longitudinal spacing relative to characteristic pier width (l/b_c).

Similarly, the maximum equilibrium scour length relative to characteristic pier width (l_{se}/b) can be expressed as

$$l_{se}/b = f_2\,(l/b_c) \tag{4}$$

and for relative maximum equilibrium scour width (w_{se}/b),

$$w_{se}/b = f_3\,(l/b_c) \tag{5}$$

Combining Eqs. (4) and (5), the resulting equation can be regarded as planner surface area of the equilibrium scour hole (a_{se}/b^2) in non-dimensional form.

$$a_{se}/b^2 = f_4\,(l/b_c) \tag{6}$$

or,

$$a_{se}/a_c = f_5\,(l/b_c) \tag{7}$$

where a_c is equal to characteristic area of the pier (πb_c^2).

Further, combining Eqs. (4), (5), and (6), a new non-dimensional term known as dimensionless volume of equilibrium scour hole ($\forall_{se}/b^3$) can be introduced.

$$\forall_{se}/b^3 = f_6\,(l/b_c) \tag{8}$$

or,

$$\forall_{se}/\forall_c = f_7\,(l/b_c) \tag{9}$$

where $\forall_c$, equal to ha_c, is the volume immersed pier above bed level.

3.2 Analysis of Scouring Parameters

Results of present investigation on scour at two eccentric piers are revealed in Figs. 6, 7, 8, 9, 10, 11 and 12.

3.2.1 Scour Depth

The scour depth of the front (reference) pier is obviously influenced by the spacing of the piers. From the scour depth analysis, it is observed that rate of change of maximum equilibrium scour depth at the front pier with respect to relative longitudinal spacing ($\mathrm{d}d_{sf}/\mathrm{d}l$) decreases with the increase in the relative spacing l/b. For square and triangular piers, $\mathrm{d}d_{sf}/\mathrm{d}l$ becomes almost constant ($\approx$1.33) more rapidly than for the circular pier. In case of square pier, if l increases then d_{sf} becomes a maximum of 33 % larger than d_{ss}. The front pier is not influenced by the rear pier when the two piers are very separated ($l/b \approx 7.5$). However, it is also noted that the magnitude of d_{sf} will be independent of l when $l > L$. For the triangular pier, the rate of increase in d_{sf}/d_{ss} with respect to the l/b_{cf} is initially slightly higher than for the circular pier, whereas it is much lower than for the square pier. But for the square pier, it becomes almost independent of the relative characteristics spacing when $l/b_{cf} \approx 5.5$. That is, the front square pier is not influenced by the rear square pier when the two piers are extremely separated ($l/b_{cf} \approx 5.5$).

The dimensionless maximum equilibrium scour depth at the front pier d_{sf} relative to pier width b is also plotted as a function of the relative spacing l/b and relative characteristic front pier spacing l/b_{cf} in Figs. 6a, b. From Fig. 6a–b, it is observed that the square pier spacing becomes insignificant when $l/b_{cf} \approx 8$ and $l/b \approx 5$. The maximum values of d_{sf} are found equal to $0.9b$ approximately. The rate of change

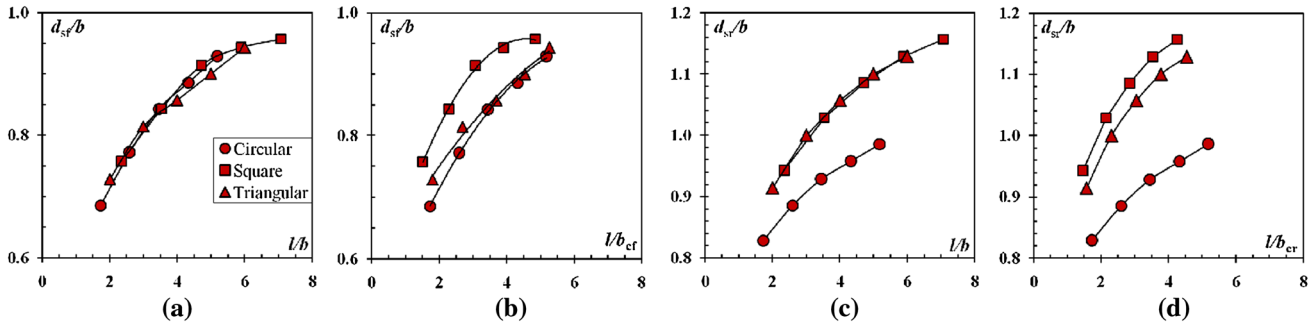

Fig. 6 Variations of **a** d_{sf}/b with l/b, **b** d_{sf}/b with l/b_{cf}, **c** d_{sr}/b with l/b and **d** d_{sr}/b with l/b_{cr}

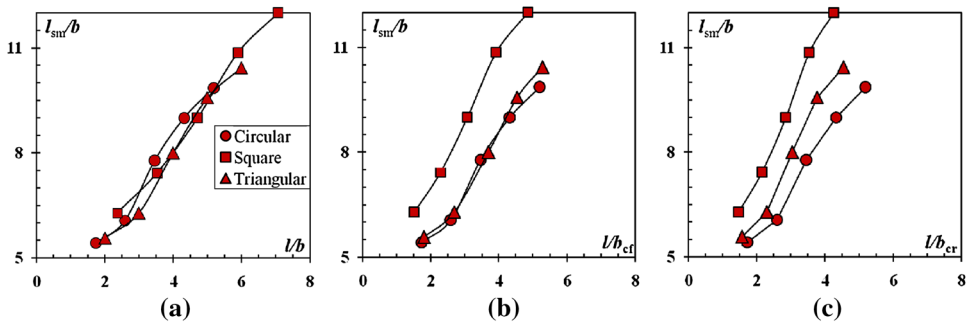

Fig. 7 Variations of l_{sm}/b with a l/b, b l/b_{cf}, and c l/b_{cr}

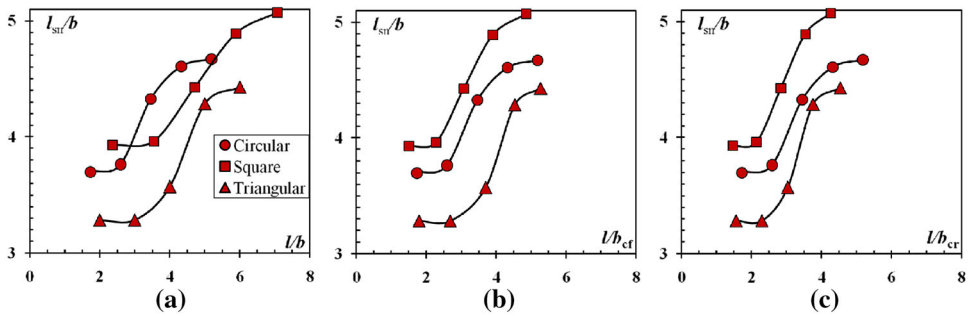

Fig. 8 Variations of l_{sn}/b with **a** l/b, **b** l/b_{cf} and **c** l/b_{cr}

of d_{sf}/b with respect to l/b that is $\mathrm{d}d_{sf}/\mathrm{d}l$ decreases as the longitudinal spacing between the piers increases. Figure 6b depicts the change of d_{sf} more understandably compared to Fig. 6b. In Fig. 6b, the magnitude d_{sf}/b for the triangular pier is always slightly higher than the magnitude of d_{sf}/b for the circular pier, whereas it is much lower than the magnitude of d_{sf}/b for the square pier.

The dimensionless maximum equilibrium scour depth at the rear pier d_{sr} is plotted as a function of the relative spacing l/b and relative rear pier characteristic spacing l/b_{cr} in Fig. 6c, d. Figure 6c indicates rate of change of maximum equilibrium scour depth at the rear pier with respect to relative spacing $\mathrm{d}d_{sr}/\mathrm{d}l$. For all the piers, $\mathrm{d}d_{sr}/\mathrm{d}l$ decreases gradually as the longitudinal spacing between the piers increases.

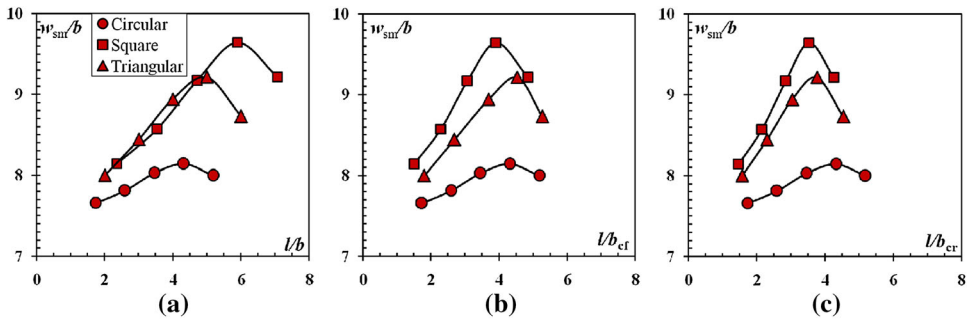

Fig. 9 Variations of w_{sm}/b with **a** l/b, **b** l/b_{cf} and **c** l/b_{cr}

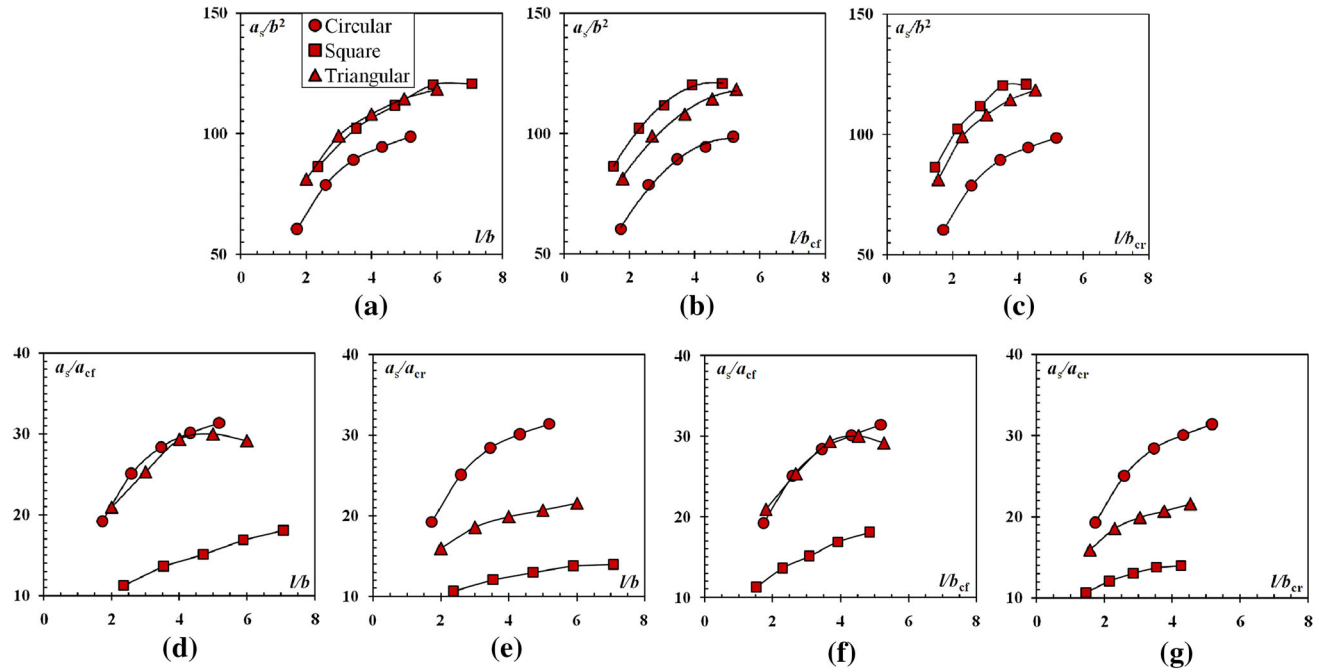

Fig. 10 Variations **a** a_s/b^2 with l/b, **b** a_s/b^2 with l/b_{cf}, **c** a_s/b^2 with l/b_{cr}, **d** a_s/a_{cf} with l/b, **e** a_s/a_{cr} with l/b, **f** a_s/a_{cf} with l/b_{cf} and **g** a_s/a_{cr} with l/b_{cr}

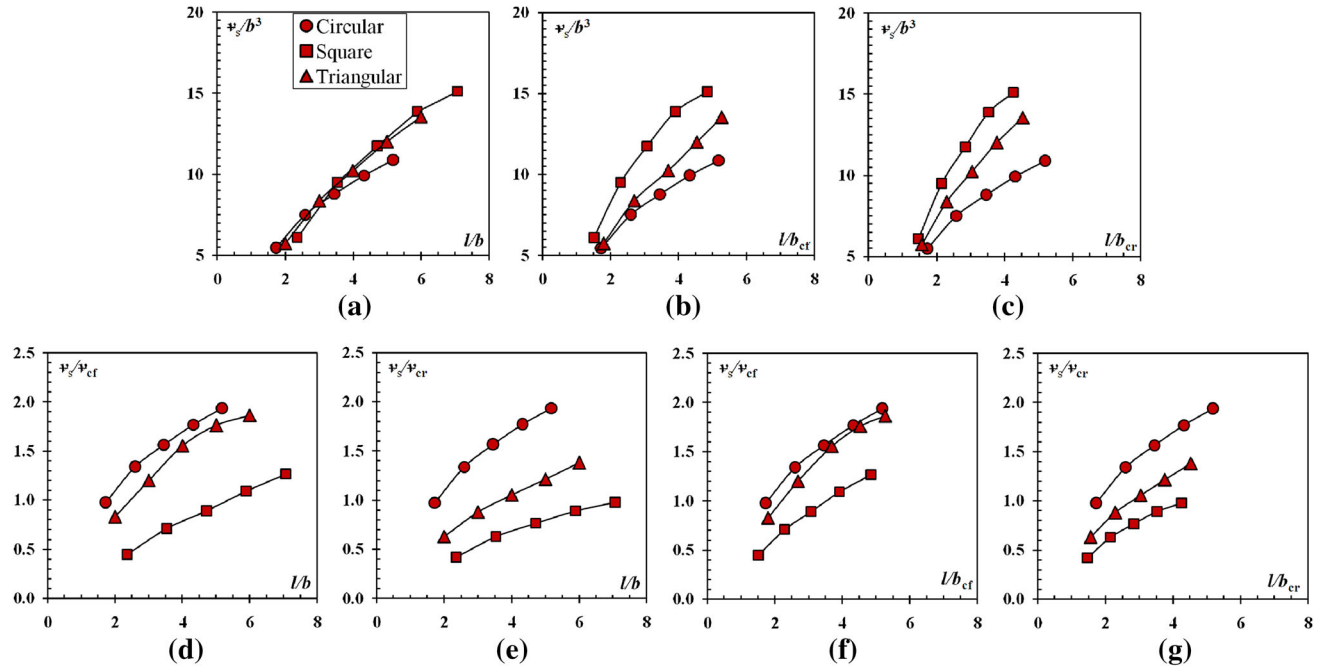

Fig. 11 Variations of **a** Ψ_s/b^3 with l/b, **b** Ψ_s/b^3 with l/b_{cf}, **c** Ψ_s/b^3 with l/b_{cr}, **d** Ψ_s/Ψ_{cf} with l/b, **e** Ψ_s/Ψ_{cr} with l/b, **f** Ψ_s/Ψ_{cf} with l/b_{cf} and **g** Ψ_s/Ψ_{cr} with l/b_{cr}

For square and triangular piers, dd_{sr}/dl may become constant ($\approx$1.75) when more rapidly compared to the circular pier. In case of square pier, d_{sr} may be found maximum 75 % larger than d_{ss} if the longitudinal spacing l increases. It is also noted that the magnitude of d_{sr} is independent of l when $l > L$ and its magnitude is equal to d_{ss}. Figure 6d shows that for the triangular pier, the rate of increase in d_{sr}/b with respect to l/b_{cr} is always much higher than for the circular pier, whereas it is lower than for the square pier.

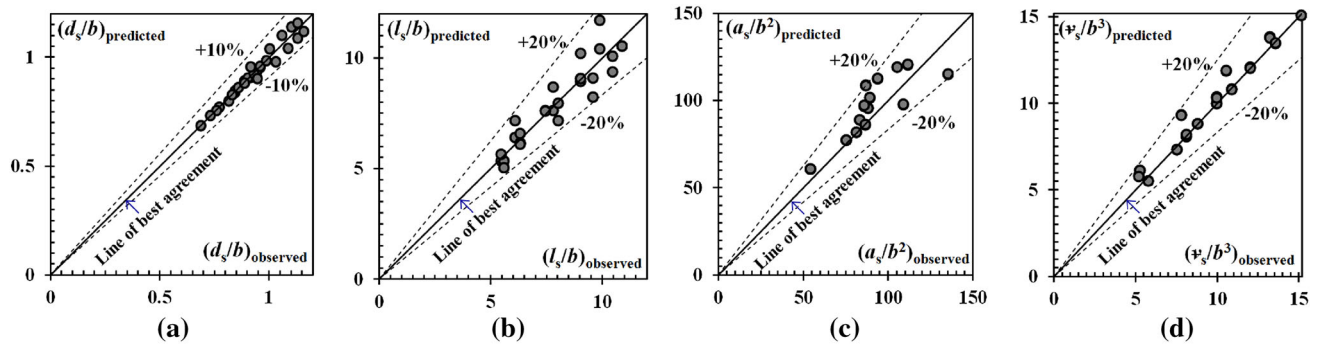

Fig. 12 Comparison between observed and predicted values of equilibrium **a** depths, **b** lengths, **c** areas, and **d** volumes of the scour holes

3.2.2 Scour Length

The dimensionless maximum equilibrium scour length l_{sm}/b is plotted as function of the relative spacing l/b, relative front pier characteristic spacing l/b_{cf}, and relative rear pier characteristic spacing l/b_{cr} in Fig. 7a–c. In Fig. 7a–c, hence, l_{sm} is non-dimensionalized by the pier width b. From Fig. 7a–c, it is observed that all the trendlines are almost similar. From Fig. 7c for the triangular pier, it is depicted that the rate of increase in l_{sm} with respect to the increase in relative spacing l is lower than for the square pier, whereas it is higher than for the circular pier.

The maximum equilibrium net scour length $l_{sn}(= l_{sm} - l)$ is shown as a function of l/b, l/b_{cf}, and l/b_{cr} in Fig. 8a–c. In Fig. 8a–c, l_{sn} is non-dimensionalized by b. From Fig. 8a, it is observed that the magnitudes of dl_{sn}/dl increase rapidly when $2.5 \leq l/b \leq 3.5, 3 \leq l/b \leq 5$ and $3.5 \leq l/b \leq 6$ for circular pier, triangular pier, and square pier, respectively. From Fig. 8b, it is illustrated that the magnitude of dl_{sn}/dl increases rapidly when $2.5 \leq l/b_{cf} \leq 3.5, 2.7 \leq l/b_{cf} \leq 4.5$ and $2.3 \leq l/b_{cf} \leq 4$ for circular, triangular and square piers, respectively. Similarly from Fig. 8c, it is depicted that the magnitude of dl_{sn}/dl increases rapidly when $2.5 \leq l/b_{cr} \leq 3.5, 2.3 \leq l/b_{cr} \leq 4$ and $2.3 \leq l/b_{cr} \leq 3.6$ for circular, triangular and square piers, respectively. It is also noted that the magnitude of l_{sn} for the triangular pier is almost always lower than the magnitude of l_{sn} for the circular and square piers.

3.2.3 Scour Width

Figure 9a–c shows the maximum equilibrium scour width w_{sm} as a function of l/b, l/b_{cf}, and l/b_{cr}. In Fig. 9a–c, w_{sm} is non-dimensionalized by b. From Fig. 9a–c, it is revealed that w_{sm} increases for a certain increase in longitudinal spacing l, but then it decreases. From Fig. 9a, it is observed that the magnitude of w_{sm}/b increases rapidly when l is approximately less than $4b$, $5b$, and $6b$ for circular, triangular, and square piers, respectively. The magnitude of w_{sm}/b decreases beyond the range. From Fig. 9b, it is noticed that the magnitude of w_{sm}/b increases rapidly when longitudinal spacing l is approximately less than $4.3b_{cf}$, $4.5b_{cf}$, and $4b_{cf}$ for circular, triangular and square piers, respectively. Then the magnitude of w_{sm}/b decreases.

Similarly from Fig. 9c, it is depicted that the magnitude of w_{sm}/b increases rapidly when l is approximately less than $4.5b_{cr}$, $4b_{cr}$, and $3.8b_{cr}$ for circular, triangular, and square piers, respectively. And then these trends are in decreasing order. It is revealed that the rate of increase in w_{sm}/b for the triangular pier is always lower than for the square piers, but higher than for the circular pier. Therefore, the rate increase in sediment transport is found maximum when l is approximately equal to $4b$, $5b$, and $6b$ for circular, triangular, and square piers, respectively. From Fig. 9a–c, it is observed that for the different longitudinal spacings, the magnitude of w_{sm} for the triangular pier is lower than the magnitude of w_{sm} for square pier, whereas it is higher than the magnitude of w_{sm} for circular pier.

3.2.4 Scour Area

Figure 10a–g displays the dimensionless planner surface area of the equilibrium scour hole (a_s) as a function of the relative spacing l/b and relative characteristic spacings l/b_{cf} and l/b_{cr}. It is revealed from Fig. 10a–g that a_s increases as the longitudinal spacing l increases. From Fig. 10a–c, it is observed that for the triangular pier, the magnitude of a_s for the different spacings is lower than for the square pier, whereas it is higher than for the circular pier. Figure 10a–c implies that da_s/dl is much higher for the circular pier compared to the triangular and square piers because the characteristic cross-sectional area of the rear circular pier a_{cr} is lowest.

From Fig. 10a–c, it is depicted that rate of increase in planner surface area of the equilibrium scour hole with respect to longitudinal spacing (da_s/dl) decreases as the longitudinal spacing between the piers as l increases. The magnitude of a_s increases rapidly up to when l is approximately equal to

5b, 6b, and 7b for the circular, triangular, and square piers, respectively, and then it decreases gradually. From Fig. 10a–c, it is also observed that da_s/dl is maximum for the square pier compared to the circular and triangular piers since the pier width b is same for all the piers. Therefore, the square pier is the most suitable for dredging (to increase the sediment transport) purpose compared to the circular and triangular piers of same width. It must be noted that the magnitude of a_s will be independent of l when $l > L$ and its magnitude will be equal to the planner surface area of the equilibrium scour hole for single pier, a_{ss}.

From Fig. 10d–g, it is observed that the rate of change of da_s/da_{cf} and da_s/da_{cr} decreases if longitudinal spacing is increased. The magnitudes of a_{cf} and a_{cr} for the square pier are much higher than the magnitudes of a_{cf} and a_{cr} for the circular and triangular piers. For this reason, the magnitudes of a_s/a_{cf} and a_s/a_{cr} for the square pier are always found lower than the magnitudes of a_s/a_{cf} and a_s/a_{cr} for the circular and triangular piers. It is also noticed that the magnitude of a_s/a_{cf} for the triangular pier decreases when $l \geq 4b$. From Fig. 10e, g it is observed that the rate of increase in a_s/a_{cr} for the square and circular piers is proportional, whereas for circular piers, it increases at a higher rate than the others.

3.2.5 Scour Volume

For the sake of comparison, dimensionless volume of the equilibrium scour hole ($\forall_s$) is plotted with the ratio of longitudinal spacing to the pier width l/b, characteristic pier width of the front pier l/b_{cf}, and characteristic pier width of the rear pier l/b_{cr} in Fig. 11a–g.

It is observed from Fig. 11a–g that $\forall_s$ increases as the longitudinal spacing l increases. From Fig. 11b, c, it is also observed that for the different spacings, the magnitude of $\forall_s$ for the triangular pier is lower than for the square pier, whereas it is higher than for the circular pier. Figure 11a–g indicates that rate of change of volume of the equilibrium scour hole with respect to longitudinal spacing $d\forall_s/dl$ decreases as the longitudinal spacing between the piers l increases. It is observed that rate of change of $d(\forall_s/\forall_p)/dl$ is much higher for the triangular pier compared to the circular and square piers as the pier volume inside the equilibrium scour hole $\forall_p$, equal to $d_{sm}a_p$, is much lower for the triangular pier compared to other piers. Figure 11d–g implies that $d(\forall_s/\forall_c)/dl$ is much higher for the circular pier compared to the triangular and square piers since the characteristic pier volume inside the equilibrium scour hole $\forall_c$ is lowest for the circular pier compared to other piers.

From Fig. 11b, c, it is revealed that $d\forall_s/dl$ is maximum for the square pier compared to the circular and triangular piers since the pier width b is same for all the piers. Therefore, the square pier is the most appropriate for dredging (to increase the sediment transport) purpose compared to the circular and triangular piers of same width, whereas the circular pier is the best alternative to reduce the bridge pier scour compared to triangular and square pier. It must be noted that the magnitude of $\forall_s$ will be independent of l when $l > L$, and its magnitude will be equal to the volume of the equilibrium scour hole for single pier $\forall_{ss}$. Figure 11a–g also indicates that the magnitude of $\forall_s$ will increase at a reasonable rate if the longitudinal pier spacing is increased further.

3.2.6 Impact of Pier Spacing on Sediment Movement

From the scour area and volume obtained with the help of surfer software, it is evident that the pier combination ($l = 0.75L$) gives more scour volume, i.e., removes more sediment from the bed compared to the other pier combinations. Hence, the combination $0.75L$ can be considered as more efficient, when more sediment removal is required from around the bridge piers. The deposition occurring downstream of the pier combinations is also examined. In the present study, the line passing through the centerline of the front and rear piers is considered as the centerline. As seen from the surface contours (Figs. 2, 3, 4, 5), the bed surface is not symmetrical about the centerline. It is observed from Figs. 2, 3, 4, and 5 that the sand deposition is more below the centerline (i.e., on the side where the eccentric pier is located) in all the two-pier tests.

From the scour width obtained with the help of surfer software, it is evident that the pier combination ($l = 0.625L$) gives more scour width, i.e., shifts more sediment toward the wall of the flume compared the other longitudinal spacings. Hence, the combination $0.625L$ can be considered as more efficient, when more increase in self-dredging is required from around the two eccentric bridge piers.

Therefore, it can be concluded that the sediment is removed from the vicinity of the two-pier group and deposited downstream on the side of the eccentric pier location. Diversion angles of scour and diversion angles of sand depositions may be observed in Figs. 2, 3, 4, and 5. It is evident that the diversion angle is more on the side where the eccentric pier is located. This phenomenon is true for all the tests carried out in the present study. Hence, this mechanism may be utilized as a dredging mechanism where the sediment can be removed downstream and deposited on the side of the bank. This phenomenon may help in maintaining a deep narrow channel which can help in inland navigation in rivers and channels.

3.2.7 Equations

For the sake of practical applications, regression equations for these dimensionless parameters with relatively high correlation coefficients, $r^2 (\approx 0.99)$, are as follows:

For square pier,

$$d_{sf}/b = -0.021\,(l/b_{cf})^2 + 0.194\,(l/b_{cf}) + 0.512 \quad (10)$$

$$d_{sr}/b = -0.019\,(l/b_{cr})^2 + 0.187\,(l/b_{cr}) + 0.713 \quad (11)$$

$$l_{sm}/b = -0.049\,(l/b_{cf})^2 + 2.095\,(l/b_{cf}) + 3.106$$
$$= 0.019\,(l/b_{cr})^2 + 2.022\,(l/b_{cr}) + 3.175 \quad (12)$$

$$a_s/b^2 = -3.64\,(l/b_{cf})^2 + 33.482\,(l/b_{cf}) + 44.197$$
$$= -4.744\,(l/b_{cr})^2 + 39.566\,(l/b_{cr}) + 38.625 \quad (13)$$

$$\forall_s/b^3 = -0.555\,(l/b_{cf})^2 + 6.211\,(l/b_{cf}) - 1.955$$
$$= -0.678\,(l/b_{cr})^2 + 7.092\,(l/b_{cr}) - 2.779 \quad (14)$$

For triangular pier,

$$d_{sf}/b = -0.006\,(l/b_{cf})^2 + 0.101\,(l/b_{cf}) + 0.573 \quad (15)$$

$$d_{sr}/b = -0.017\,(l/b_{cr})^2 + 0.176\,(l/b_{cr}) + 0.682 \quad (16)$$

$$l_{sm}/b = 0.09\,(l/b_{cf})^2 + 0.841\,(l/b_{cf}) + 3.636$$
$$= 0.001\,(l/b_{cr})^2 + 1.756\,(l/b_{cr}) + 2.629 \quad (17)$$

$$a_s/b^2 = -2.518\,(l/b_{cf})^2 + 28.082\,(l/b_{cf}) + 39.737$$
$$= -4.006\,(l/b_{cr})^2 + 36.575\,(l/b_{cr}) + 34.452 \quad (18)$$

$$\forall_s/b^3 = -0.127\,(l/b_{cf})^2 + 3.088\,(l/b_{cf}) + 0.718$$
$$= -0.315\,(l/b_{cr})^2 + 4.519\,(l/b_{cr}) - 0.509 \quad (19)$$

For circular pier,

$$d_{sf}/b = -0.011\,(l/b_{cf})^2 + 0.145\,(l/b_{cf}) + 0.489 \quad (20)$$

$$d_{sr}/b = -0.007\,(l/b_{cr})^2 + 0.092\,(l/b_{cr}) + 0.691 \quad (21)$$

$$l_{sm}/b = -0.007\,(l/b_c)^2 + 1.411\,(l/b_c) + 2.843 \quad (22)$$

$$a_s/b^2 = -3.23\,(l/b_c)^2 + 33.009\,(l/b_c) + 13.65 \quad (23)$$

$$\forall_s/b^3 = -0.224\,(l/b_c)^2 + 3.08\,(l/b_c) + 0.879 \quad (24)$$

As the literature lacks equations of similar context of those presented by Eqs. (10) through (24), the accuracy of these equations cannot be verified directly at this stage. However, in future the measured equilibrium depths, lengths, areas, and volumes of the scour holes can be compared with these empirical Eqs. (10–24) as these are in dimensionless form. Some parameters like approach flow depth, particle size and inflow velocity are not varied in this research. In prospect these parameters may be varied with the change of longitudinal pier spacing and characteristic pier width to make these empirical equations in more generalized form. These empirical equations may be utilized as useful tool not only to promote the related studies of scour parameters around multi-pier arrangements, but also to give importance two parameters—longitudinal pier spacing and characteristic pier width for design and analysis of sediment transport in future.

Results of the comparative analyses are depicted in Fig. 12a–d. Figure 12a shows a comparison of observed and predicted values of dimensionless equilibrium scour depth for all tests. It may be seen from Fig. 12a that Eq. (10) gives less than ±10 % error for all the data. Therefore, the calculated scour depth matches very well with the measured data.

It can be seen from Fig. 12b–d that the deviation between the predicted and measured data are mostly in a range of –20 to 20 %, which is the calculated dimensionless equilibrium lengths, areas, and volumes of the scour holes matches well with the observed data. Therefore, one can use Eqs. 10-24 for the practical prototype applications. These equations require selection of appropriate design parameters to be used in the dimensionless longitudinal spacing to the characteristic pier width term. The corresponding depths, lengths, areas, and volumes of the scour holes can then be obtained using respective equations. Since the volume of the scour hole gives the amount of bed material eroded from the surrounding of the eccentric piers, it can give some clues about the depth of the protection area around the eccentric bridge piers. On the other hand, the sizes of the surface area of the scour holes dictate the extension of the armoring countermeasure around the bridge piers.

As a concluding remark, it should be emphasized, however, that the additional experiments need to be conducted using different bed materials and flow conditions to generalize the design details of scour geometry and the armoring countermeasure.

4 Concluding Remarks

The equilibrium scour geometry around two circular, square, and equilateral triangular piers, positioned in in-line front and eccentric rear arrangement, is determined by carrying out 19 clear water scour tests. Here the eccentricity was kept constant with the varying longitudinal spacing from 0.25, 0.375, 0.5, 0.625, and 0.75 times the maximum equilibrium scour-affected length for a single-pier test. At $l = 0.75L$, the maximum scour depth at the eccentric rear pier is found about 45–60 % greater than that in the single-pier case. In addition, at l equal to $0.75L$, the maximum depth of the scour hole at the upstream of in-line front pier is about 35 % more than at the single-pier case. The reason may be the effect of reinforcing scour mechanism [10]. The pier arrangement and the interference between the horseshoe vortex of the rear pier and wake vortex of the front pier may also play an important role in the creation and formation of the greater scour depth at the eccentric rear piers.

Graphs have been plotted between the maximum equilibrium scour depth, length, and width with respect to the longitudinal spacing. The rate of change of planner surface area and the volume of the equilibrium scour holes was also observed relative to the change of longitudinal spacing. For the two-pier tests, initially the rate of spatial changes of maximum scour depth, length, planner surface area, and vol-

ume increase if the longitudinal spacing between the piers is increased, but then it decreases. The magnitude of net scour length l_{sn} for the triangular pier is found almost always lower than the magnitude of l_{sn} for the circular and square piers. For circular, triangular, and square piers, the relative spacing l/b and relative characteristic spacings l/b_{cf} and l/b_{cr} are found to be the most effective to enhance the sediment transport mechanism when l/b is almost equal to 4, 5, and 6 and l/b_{cr} is almost equal to 4, 4, and 3.8, respectively. Moreover, it was also found that we end up generating the greatest scour hole when the circular-shaped piers are replaced by equilateral triangular piers and then by square piers of same width with all the other conditions remaining same. Thus, it can be concluded that with $3b$ eccentricity and longitudinal spacing within a fraction of L, the scour at the rear pier gets enhanced.

The diversion angle of the scour and also the deposition is more on the side of the eccentric pier. It indicates that the sediment, removed from the flume or open-channel bed, is deposited on one side of the channel. This finding is significant as it proves that the transported sediment load in a river or open channel can be shifted toward the bank by self-dredging with the help of suitable two-pier combination, eccentricity and longitudinal spacing.

The experimental data of this study may be used as a useful data bank not only to promote the related studies of scour parameters around multi-pier arrangements, but also to validate the results obtained by numerical simulations. As a final remark, the equations proposed in this study (Eqs. 10–24) are assumed to provide preliminary design guidelines for determining the local scour characteristics around two eccentric piers of different shapes required for bridge piers and self-dredging. Additional experimental research is recommended to further verify these equations.

References

1. Breusers, H.N.C.; Nicollet, G.; Shen, H.W.: Local scour around cylindrical piers. J. Hydraul. Res. **15**(3), 211–252 (1977)
2. Raudkivi, A.J.; Ettema, R.: Clear-water scour at cylindrical piers. J. Hydraul. Eng. **109**(3), 338–350 (1983)
3. Melville, B.W.: Local scour at bridge abutments. J. Hydraul. Eng. **118**(4), 615–631 (1992)
4. Dey, S.: Local scour at piers, part 1: a review of development of research. Int. J. Sediment. Res. **12**(2), 23–44 (1997)
5. Hoffmans, G.J.C.M.; Verheij, H.C.: Scour Manual. A.A. Balkema, Rotterdam (1997)
6. Melville, B.W.; Coleman, S.E.: Bridge Scour. Water Resources Publications, LLC, Colorado (2000)
7. Ataie-Ashtiani, B.; Beheshti, A.A.: Experimental investigation of clear-water local scour at pile groups. J. Hydraul. Eng. **132**(10), 1100–1104 (2006)
8. Khwairakpam, P.; Ray, S.S.; Das, S.; Das, R.; Mazumdar, A.: Scour hole characteristics around a vertical pier under clear water scour conditions. ARPN J. Eng. Appl. Sci. **7**(6), 649–654 (2012)
9. Das, S.; Ghosh, R.; Das, R.; Mazumdar, A.: Clear water scour geometry around circular piers. Ecol. Environ. Conserv. **20**(2), 479–492 (2014)
10. Breusers, H.N.C; Raudkivi, A.J.: Scouring, IAHR Design Manual. A.A. Balkema, Rotterdam (1991)
11. Richardson, E.V.; Lagasse, P.F.: Stream Stability and Scour at Highway Bridges. ASCE, Tennessee (1998)
12. Gaudio, R.; Tafarojnoruz, A.; De, B.S.: Sensitivity analysis of bridge pier scour depth predictive formulae. J. Hydroinform. **15**(3), 939–951 (2013)
13. Melville, B.W.: Local Scour at Bridge Sites. Report 117. School of Eng., Univ. of Auckland, New Zealand (1975)
14. Dargahi, B.: Controlling mechanism of local scouring. J. Hydraul. Eng. **116**(10), 1197–1214 (1990)
15. Michael, S.A.; Mohamed, G.M.; Mohamed, S.B.A.M.: Wake vortex scour at bridge piers. J. Hydraul. Eng. **117**(7), 891–904 (1991)
16. Coleman, S.E.: Clearwater local scour at complex piers. J. Hydraul. Eng. **131**(4), 330–334 (2005)
17. Ashtiani, A.B.; Ghorghi, B.Z.; Beheshti, A.A.: Experimental investigation of clear-water local Scour of compound piers. J. Hydraul. Eng. **136**(6), 343–351 (2010)
18. Das, S.; Ghosh, S.; Mazumdar, A.: Kinematics of horseshoe vortex in a scour hole around two eccentric triangular piers. Int. J. Fluid Mech. Res. **41**(4), 296–317 (2014)
19. Das, R.; Khwairakpam, P.; Das, S.; Mazumdar, A.: Clear-water local scour around eccentric multiple piers to shift the Line of sediment deposition. Asian J. Water Environ. Pollut. **11**(3), 47–54 (2014)
20. Sumner, D.; Wang, S.S.T.; Price, S.J.; Paidoussis, M.P.: Fluid behavior of side-by-side circular cylinders in steady cross-flow. J. Fluids Struct. **13**(3), 309–338 (1999)
21. Akilli, H.; Akar, A.; Karakus, C.: Flow characteristics of circular cylinders arranged side-by-side in shallow water. Flow Meas. Inst. **15**(4), 187–189 (2004)
22. Elliott, K.R.; Baker, C.J.: Effect of pier spacing on scour around bridge piers. J. Hydraul. Eng. **111**(7), 1105–1109 (1985)
23. Raudkivi, A.J.: Loose Boundary Hydraulics. A.A. Balkema, Rotterdam (1998)
24. Graf, W.H.: Fluvial Hydraulics, Flow and Transport Processes in Channels of Simple Geometry. Wiley, Great Britain (2003)
25. Das, S.; Das, R.; Mazumdar, A.: Comparison of characteristics of horseshoe vortex at circular and square piers. Res. J. Appl. Sci. Eng. Technol. **5**(17), 4373–4387 (2013)
26. Das, S.; Das, R.; Mazumdar, A.: Circulation characteristics of horseshoe vortex in scour region around circular piers. Water Sci. Eng. **6**(1), 59–77 (2013)
27. Das, S.; Midya, R.; Das, R.; Mazumdar, A.: A study of wake vortex in the scour region around a circular pier. Int. J. Fluid. Mech. Res. **40**(1), 42–59 (2013)
28. Das, S.; Das, R.; Mazumdar, A.: Variations of clear water scour geometry at piers of different effective widths. Turkish J. Eng. Environ. Sci. **38**(1), 97–111 (2014)
29. Yalin, M.S.: Mechanics of Sediment Transport. Pergamon, NY (1977)